nature geoscience

ARTICLES

https://doi.org/10.1038/s41561-019-0329-3

Interruption of two decades of Jakobshavn Isbrae acceleration and thinning as regional ocean cools

Ala Khazendar[1]*, Ian G. Fenty[1], Dustin Carroll[1], Alex Gardner[1], Craig M. Lee[2], Ichiro Fukumori[1], Ou Wang[1], Hong Zhang[1], Hélène Seroussi[1], Delwyn Moller[3], Brice P. Y. Noël[4], Michiel R. van den Broeke[4], Steven Dinardo[1] and Josh Willis[1]

Jakobshavn Isbrae has been the single largest source of mass loss from the Greenland Ice Sheet over the last 20 years. During that time, it has been retreating, accelerating and thinning. Here we use airborne altimetry and satellite imagery to show that since 2016 Jakobshavn has been re-advancing, slowing and thickening. We link these changes to concurrent cooling of ocean waters in Disko Bay that spill over into Ilulissat Icefjord. Ocean temperatures in the bay's upper 250 m have cooled to levels not seen since the mid 1980s. Observations and modelling trace the origins of this cooling to anomalous wintertime heat loss in the boundary current that circulates around the southern half of Greenland. Longer time series of ocean temperature, subglacial discharge and glacier variability strongly suggest that ocean-induced melting at the front has continued to influence glacier dynamics after the disintegration of its floating tongue in 2003. We conclude that projections of Jakobshavn's future contribution to sea-level rise that are based on glacier geometry are insufficient, and that accounting for external forcing is indispensable.

Jakobshavn Isbrae, also known as Sermeq Kujalleq, in central west Greenland (Fig. 1a,b) is the ice sheet's fastest glacier[1] and its largest by volume discharge[2]. For two decades, it exhibited a persistent pattern of frontal retreat, flow acceleration and thinning[3–7]. Between 2003 and 2016, the surface of the lower reaches of the glacier dropped by ~160 m (Supplementary Figs. 1 and 2). The destabilization of Jakobshavn Isbrae coincided with the intrusion in 1997 of warmer waters into Disko Bay[8]. Higher melting at the base of Jakobshavn's floating tongue was hypothesized to have contributed to its thinning and eventual disintegration[9–11] in May of 2003[12]. The glacier's acceleration and thinning have been interpreted as a dynamic response to the reduction of basal and lateral drag that oppose the gravitational driving stress near the glacier front as it retreated[13–15]. Response to the perturbation at the front propagates far inland[16–19] (Figs. 1c and 2 and Supplementary Figs. 2 and 3). Since the late 1990s, Jakobshavn developed Greenland's largest cumulative ice discharge anomaly[7], contributing the equivalent of ~0.9 mm to global mean sea-level rise between 2000 and 2010[14].

The evolution of Jakobshavn Isbrae is therefore of consequence to the magnitude of Greenland's future mass loss and contribution to sea-level rise. The glacier has been viewed as a strong candidate for continued retreat given the decadal persistence of its acceleration and thinning, its deep trough that extends up to 200 km inland[20] and its retrograde bed that portends self-sustaining instability[1,14,16,19,21,22]. Here we provide evidence that, at least temporarily, this retreat has halted in response to regional ocean cooling.

The slowing and thickening of Jakobshavn Isbrae

After nearly two decades of sustained thinning, our observations show that the thinning rates of Jakobshavn Isbrae slowed down since 2014 and that the glacier significantly thickened between 2016 and 2017, and again between 2017 and 2018. We detect this change from the analyses of two independent National Aeronautics and Space Administration (NASA) data sets, namely, the radar altimetry of the Oceans Melting Greenland (OMG) mission[23] (Fig. 1c and Methods), and the laser altimetry of Operation IceBridge[24] (Fig. 2 and Methods). Between 2016 and 2017, we observe ice thickening of 20 to 30 m in the vicinity of the front (Fig. 2). The thickening diminishes with distance upstream over the first 30 km, beyond which the glacier experiences uniform lowering of 1 to 3 m. Repeat Glacier and Ice Surface Topography Interferometer (GLISTIN) measurements in 2018 show that the thickening continued at a similar rate near the front, but has now extended as far as 80 km upstream and has spread laterally (Fig. 2 and Supplementary Fig. 4). A similar surface elevation change pattern between 2016 and 2017 is detected by the Airborne Topographic Mapper (ATM) laser altimeter (Methods). The thickening measured by ATM in the lower parts of the glacier is higher than observed by GLISTIN (Supplementary Fig. 3), which we attribute to the continued slowing of the glacier and the net accumulation of snow on the ice between the March GLISTIN and late April to early May ATM surveys (Methods and Supplementary Table 1). The net contribution of surface processes (precipitation and melting) to observed elevation changes is a few metres per year (Supplementary Fig. 5).

The glacier surface has consistently lowered since 2003 (Fig. 2 and Supplementary Figs. 2 and 3), undergoing the largest drop in elevation between 2012 and 2013. Since 2013, however, the rate of surface lowering has lessened. Moreover, from 2014 to 2016 the concentration of the highest rates of thinning near the front has been far less pronounced compared with previous years. These two observations suggest a weakening of the dynamic component of the thinning, which is strongly supported by concurrent changes in flow speeds. The flow of Jakobshavn accelerated between 1998 and 2013 (Fig. 3b and Supplementary Fig. 6), modulated by increasing

[1]Jet Propulsion Laboratory, California Institute of Technology, Pasadena, CA, USA. [2]Applied Physics Laboratory, University of Washington, Seattle, WA, USA. [3]Remote Sensing Solutions, Barnstable, MA, USA. [4]Institute for Marine and Atmospheric Research Utrecht, Utrecht University, Utrecht, The Netherlands. *e-mail: ala.khazendar@jpl.nasa.gov

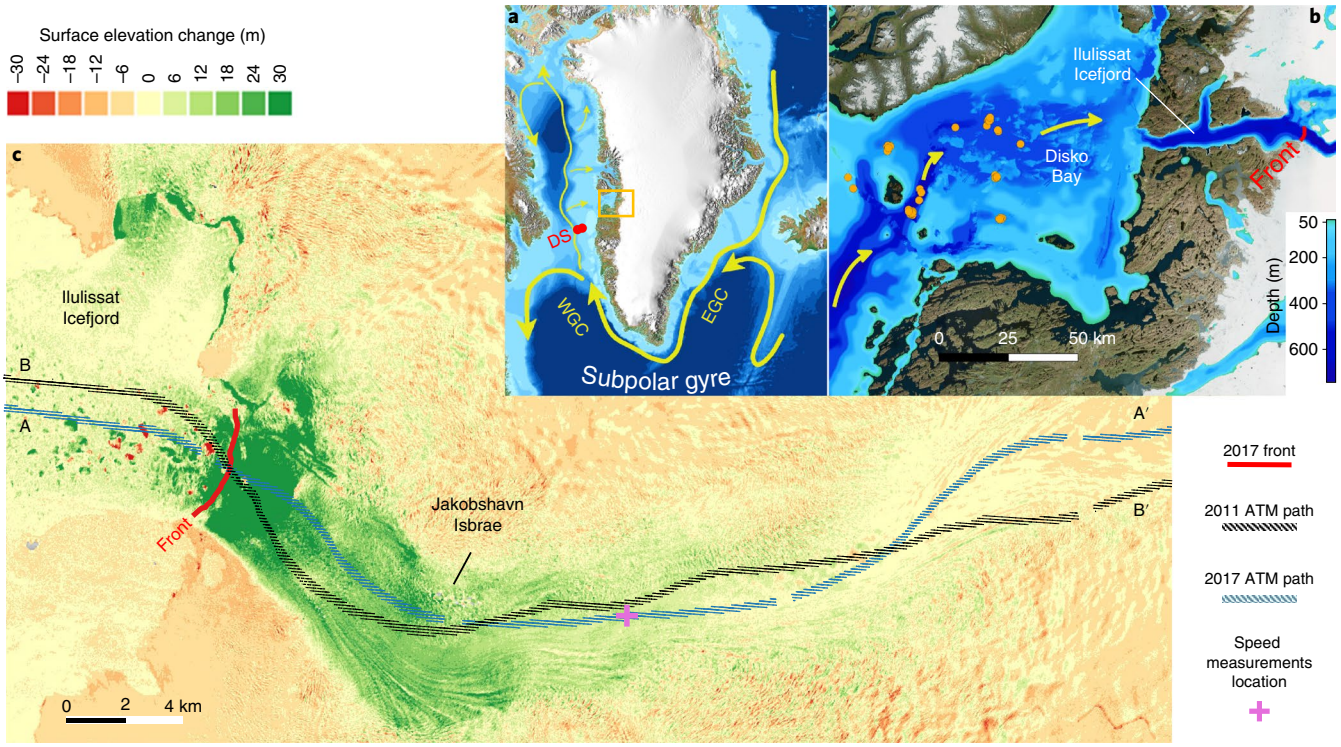

Fig. 1 | The study area and recent thickening observations. a, A map of Greenland showing the location of Jakobshavn and Disko Bay (orange box) and major ocean currents (EGC, East Greenland Current; WGC, West Greenland Current). DS denotes Davis Strait, and the two red dots mark mooring locations referred to as C5 and C6. Ocean depth below sea level (bathymetry) is shown in the blue colours (scale is in **b**). The white, hill-shaded areas are where the topography is greater than 800 m above sea level. **b**, A map of Disko Bay and part of Jakobshavn Glacier. The blue colours show the depth of the ocean and of the bed below sea level under the ice. The orange dots indicate the locations of conductivity–temperature–depth (CTD) measurements in Disko Bay. The red line indicates the location of the Jakobshavn front on 1 May 2017. The yellow arrows depict the currents carrying the warm water through Disko Bay towards Ilulissat Fjord and Jakobshavn. **c**, Generalized thickening along the main trunk, and fastest flowing part, of Jakobshavn Isbrae, detected by GLISTIN radar surveys between 2016 and 2017. The colour-saturated area near the front reflects the extent of glacier advance between the two GLISTIN measurements. ATM ground tracks are labelled AA′ for the year 2017 and BB′ for 2011. The cross marks the point at which the speed is found in Fig. 3b.

seasonal variability in the latter years. Since 2013, the year of greatest thinning, glacier speeds slowed while remaining above their pre-1998 levels. More significant slowing occurs in 2017, the first year we detect a transition from glacier thinning to thickening. Observations in spring 2018 reveal a continuation of glacier deceleration and thickening.

Recent cooling of ocean waters near Jakobshavn Isbrae

Over the past several years, ocean temperatures have cooled on the continental shelf in the vicinity of Jakobshavn Isbrae (Fig. 3d and Supplementary Figs. 7 and 8). We find that ocean temperatures in Disko Bay below about 150 m cooled by nearly 2 °C between 2014 and 2016. It is primarily water from this deeper layer that flows into Ilulissat Icefjord and comes into contact with Jakobshavn Isbrae at depth[25,26].

Atlantic Water reaches Disko Bay via a boundary current that circulates along the shelf break around Greenland's continental shelf[27] (the East and West Greenland Current, Fig. 1a). During its transit in the boundary current, Atlantic Water follows the northern periphery of the North Atlantic subpolar gyre (Fig. 1a) and cools by several degrees Celsius[28]. After flowing through Davis Strait at 67° N, a branch of the boundary current is steered northeast towards the ice sheet in a 350-m-deep trough cut into the shallower (100–250 m) continental shelf (Fig. 1b). This trough provides a pathway that permits warm, salty Atlantic Water to transit across the shelf beneath the shallower and fresher Polar Water layer[25,26]. Before reaching Jakobshavn, Atlantic Water in the trough is partially impeded by two sills, one at mid-shelf (68.50° N, 54.60° W) at ~300 m depth and another near the mouth of Ilulissat Icefjord (69.18° N, 51.25° W) at 250 m. A mixture of Atlantic and Polar waters with potential densities between 1,027.2 and 1,027.4 kg m^{-3} (Supplementary Fig. 9) flows over this last sill into Ilulissat Icefjord[26]. Flushing of the fjord happens mostly during summer, when density surfaces are shallower and subglacial discharge (Fig. 3c and Supplementary Fig. 16) drives strong circulation throughout the fjord[25].

The cooling we observe in Disko Bay is also seen at 200–250 m in instrumented moorings at two sites (Fig. 1a and Methods) situated upstream in the northward-flowing West Greenland Current in eastern Davis Strait (Fig. 3e and Supplementary Figs. 9 and 10). The close correspondence of the temperature and salinity observed in Davis Strait and in Disko Bay (Supplementary Fig. 9) supports the conclusion that the water in these density classes in Disko Bay primarily originates upstream and passes through the moorings[25,26]. These mooring data reveal anomalously cold waters persisting in Davis Strait throughout the second half of 2015, normally the warming period of the seasonal temperature cycle (Fig. 3e and Supplementary Fig. 10). The data then show cooling in the first half of 2016 of a normal magnitude (~2 °C) acting on water at already below-average temperatures cooling it to 1 °C, which is ~2–2.5 °C colder than the 2009–2015 values (Fig. 3e and Supplementary Fig. 10). The mooring data also show that temperatures remain significantly below average through summer 2017.

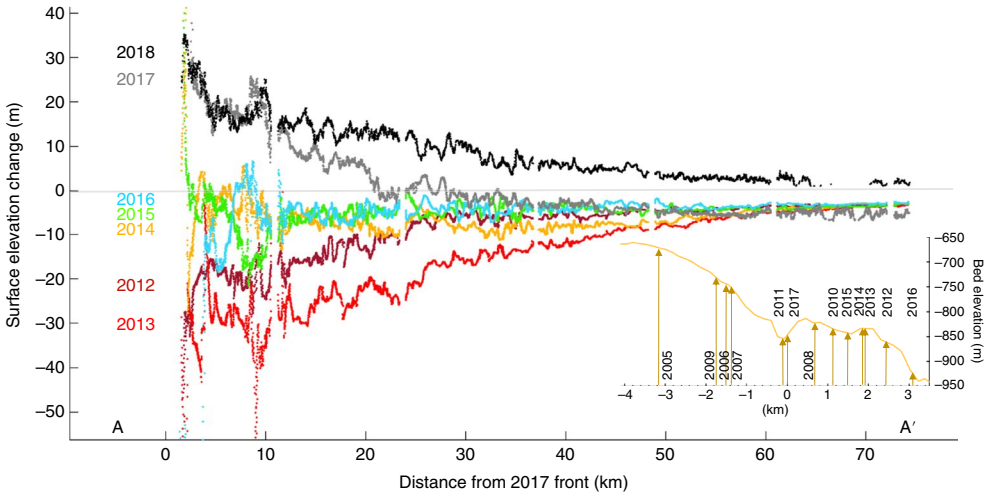

Fig. 2 | Surface elevation changes and bed depths along the main trunk of Jakobshavn. Changes in elevation for each year shown are found relative to the preceding year. The path AA′ extends ~80 km inland from the point where the 2017 ATM track intersects the front at the closest available date (Fig. 1 and Supplementary Table 1). All data are from ATM, except for the years 2017 and 2018, which are from GLISTIN (Methods). The inset depicts bed topography (relative to mean sea level) and front locations during the study period. The exact dates of the fronts are given in Supplementary Table 1.

A similar timing and magnitude of the observed Davis Strait cooling is seen in the Estimating the Circulation and Climate of the Ocean (ECCO) ocean state estimate, as well as 300 km further upstream in the boundary current at 64° N (Fig. 3e). Agreement is excellent between the mooring data and ECCO in the timing and magnitude of both the temperature and salinity (Fig. 3e and Supplementary Figs. 11 and 12a–c). Given the close agreement between the model and observations, and ECCO's dynamic and kinematic consistency, we use it to investigate the origins of the cooling. We propose that cooler Atlantic Waters entering Davis Strait from the south contributed to the observed cooling in Disko Bay as these waters form the basis of the mixture that eventually reaches the bay and Jakobshavn Isbrae. To explain the cooling observed in Davis Strait and in Disko Bay in 2015 and 2016, we first note that anomalous wintertime heat loss lowered ocean temperatures across the entire North Atlantic subpolar gyre since 2011 by about 0.6 °C on average in the top 300 m of the water column (Supplementary Fig. 13). In the northern Irminger Sea where Atlantic Water first enters the East Greenland Current, ECCO shows that average temperatures have cooled by 0.75 °C over the same time period with the greatest cooling occurring during the winter of 2015 (Supplementary Fig. 14). This 0.75 °C cooling of waters far upstream in the Irminger Sea explains part of the 2 °C cooling observed in Davis Strait and in Disko Bay. Our analysis indicates that the remaining 1.25 °C cooling signal originated from wintertime heat loss within the West Greenland Current between Cape Desolation and Davis Strait (points B and D, respectively, in Supplementary Figs. 11 and 14). In this region, wintertime mixed layers deepen and cool dramatically relative to other years (Supplementary Fig. 15), reaching temperatures as low as 1 °C at 200 m depth. The state estimate shows surface heat and buoyancy loss to the atmosphere and convective mixing in the boundary current during the winter of 2015–2016 were responsible for the largest part of the cooling at depth in Disko Bay in 2016.

The origin of the unusually cold Atlantic Water in Disko Bay in 2016 can therefore be explained by a combination of factors. The exceptional cooling of the subpolar gyre in the winter of 2015 was followed by a weak recovery of temperatures along the boundary current throughout the remainder of the year. Wintertime cooling in 2016 across the Labrador Sea including the West Greenland Current drove temperatures down further still. These exceptionally cold waters at depth were observed flowing north in the Davis Strait moorings and downstream in Disko Bay.

The transition to colder ocean temperatures in the vicinity of Jakobshavn Isbrae interrupts the period of warmer conditions that has lasted for nearly 20 years. The processes described here underline the connection between oceanic conditions in Disko Bay, the main source of Ilulissat Icefjord's water, and long-term remote climate forcing variability across the North Atlantic Ocean.

Correspondence of glacier evolution to submarine melting

As in the late 1990s, changes in the ocean emerge as the main influence on the recent slowing and thickening of Jakobshavn Isbrae. Synchronous changes in the other two large glaciers terminating in Ilulissat Icefjord further support the connection between oceanic conditions and glacier dynamic changes over the study period, which starts shortly after the disintegration of the ice shelf in 2003.

We calculate ocean-induced melting at the front (Fig. 3a and Methods) with an approach that considers subglacial freshwater discharge (surface meltwater runoff, Fig. 3c), the depth at which the subglacial discharge emerges at the grounding line (Fig. 2, inset), and ocean temperature and density stratification (Fig. 3d and Supplementary Fig. 9). These parameters have been shown to control submarine melting rates[29–31]. Water properties in the fjord link submarine melting to oceanic forcing while subglacial discharge links melting to atmospheric forcing.

The variability of the modelled frontal melting rates corresponds well to changes in ice flow and thickness. Before 2010, flow speed increased from year to year in a remarkably near-linear manner (Fig. 3b), and glacier thinning rates varied within a relatively narrow range (Fig. 3a). After that year, flow speed and changes in glacier thickness became highly variable, and both agree well with large changes in submarine melting rates. Those changes in submarine melting reflect the interplay between the variability in ocean properties and in subglacial discharge volumes. Especially salient is the increase in ocean-induced melting in 2011 and 2012 (Fig. 3a) and the concurrent jumps in flow speeds and thinning rates, both the highest recorded for Jakobshavn during the study period (Figs. 2 and 3a,b and Supplementary Fig. 2). The high melting rates were the result of higher ocean temperatures (Fig. 3d and Supplementary Figs. 7 and 8) coinciding with increased subglacial discharge during those two years (Fig. 3c). Starting in 2013, volumes of subglacial

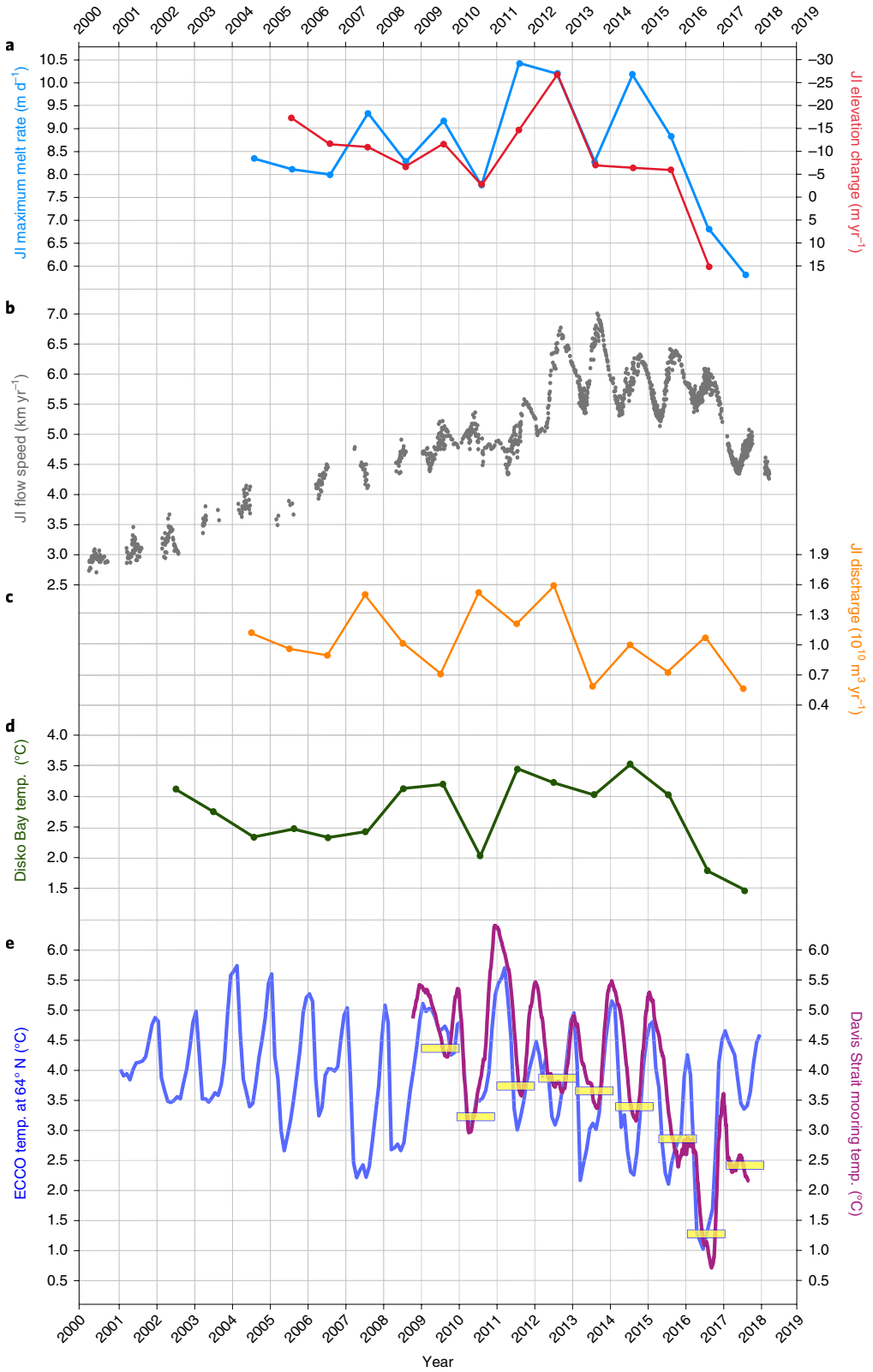

Fig. 3 | Ocean forcing and glacier response. a, Normalized changes in surface elevation of Jakobshavn Isbrae (JI) from one year to the next (red line), averaged between 10 and 15 km upstream from the front location in each year (Methods and Supplementary Table 1). Also shown is the yearly average of the maximum melting rate at the glacier front as estimated by the plume model (blue line, Methods). **b**, The flow speed of Jakobshavn at the location marked by the cross in Fig. 1. This series is extended to 1985 in Supplementary Fig. 6, which also shows data sources. **c**, Yearly integrated subglacial discharge volumes. **d**, Observed summer ocean temperatures in Disko Bay at 250 m depth. **e**, Ocean temperatures between the depths of 200 and 250 m in the West Greenland Current from moorings in eastern Davis Strait (31-day boxcar smoothed), and temperatures upstream at 64° N from the ECCO state estimate (monthly mean). Average summertime 250-m-depth ocean temperatures from the mooring are shown as yellow bars to simplify comparison with **d**.

discharge were lower, which contributed to lower melting rates in 2013 and 2015, coinciding with the slower thinning observed in 2014 and 2016 (Figs. 2 and 3a). Most prominently, the sharp drop in ocean temperatures in 2016 and 2017 by 2 °C relative to the peak temperature in 2014 corresponds to the slowing and dramatic thickening of the glacier in 2017 and 2018. The higher melting in 2014 simulated in our plume model is not reflected in flow acceleration and thinning, which we cannot explain. Despite this, the correlation coefficient between the time series of normalized surface elevation changes and melting rates is 0.67, with a P value of <0.02 (Fig. 3a).

Further compelling evidence of the origin of recent changes is the concurrent slowing and thickening of the other two large glaciers that terminate in Ilulissat Icefjord (Supplementary Fig. 1). The thickening of Jakobshavn's northern branch in its lower reaches was a few metres between 2016 and 2017, but reached 20 to 25 m between 2017 and 2018 (Supplementary Fig. 4). Avannarleq Ilulissat Glacier thinned by 5 to 7 m between 2016 and 2017 in the areas located ~4 km and farther upstream from the front, where the glacier is less crevassed and surface elevation change is easier to detect. In contrast, between 2017 and 2018 surface elevation was slightly higher or unchanged within measurement uncertainty (Supplementary Fig. 4). Time series of the flow speeds of the three glaciers from 1985 to 2018 (Supplementary Fig. 6) show remarkable similarities. The flow of the three glaciers was relatively stable during the first 15 years of the time series. Flow speeds of all three glaciers then started to increase significantly between 1998 and 2000 when warmer waters were observed in Disko Bay[8]. The glaciers started to slow down between 2014 and 2016. Such synchronicity of behaviour strongly suggests that oceanic and atmospheric forcings, shared by the glaciers, dominate their evolution over decadal timescales.

Sensitivity of glacier to external forcing and geometry

The strong correlation between changes in the glacier's flow and thickness and melting rates at its front points to submarine melting, driven by both atmospheric and oceanic forcings, as the likely principal mechanism affecting the advance and retreat of the glacier, and the consequent dynamic changes. We examine the factors that modify submarine melting, and consider other external forcings and controls that have been hypothesized to affect glacier dynamics[32].

Sensitivity experiments demonstrate the relative importance of the three main parameters that influence modelled melting rates at the front (Supplementary Fig. 17). They show that the depth at which subglacial discharge emerges has the least effect on melting rate variability, which is explained by the relatively deep grounding line. Subglacial discharge volumes, which strongly reflect atmospheric temperature variability over the glacier's drainage basin, significantly modify the melting rates. Ocean temperature, however, is the largest contributor to interannual submarine melting variability predicted for Jakobshavn Isbrae by our model. In particular, changes in subglacial discharge alone cannot explain the large drop in the melting rate of 2016 and 2017 and the corresponding rapid glacier thickening. The predominance of ocean temperature variability is to be expected in light of plume modelling studies that found submarine melting to be linearly proportional to water temperature but sub-linearly so to subglacial discharge[30,33]. We reiterate that the strongest correlation between modelled submarine melting and observed glacier thickness (Fig. 3a) is realized when both ocean properties and subglacial discharge are considered.

In addition to external oceanic and atmospheric forcings, a long-hypothesized control on the evolution of Jakobshavn Isbrae is glacier geometry, including surface height above floatation and ice thickness near the front and bed slope. Our calculations (Supplementary Tables 2 and 3) do not find a strong correspondence between those aspects and changes in flow speed and surface elevation. This seems to agree with previous findings[1] that aspects such as height above floatation and water depth can explain seasonal variability in glacier dynamics, but are less pertinent on longer timescales.

Our analyses cannot exclude the possibility of other mechanisms affecting glacier behaviour. The roles of ice mélange on interannual timescales[4,34–36], and that of cryo-hydrologic warming[37,38], have yet to be elucidated. Both processes are discussed further in the Supplementary Information. We nonetheless find the evidence sufficient to conclude that ocean temperature variability, through its influence on submarine melting rates, has been a main, and sometimes dominant, factor in shaping Jakobshavn Isbrae's interannual dynamic evolution since the disintegration of the ice shelf in 2003. The principal role of oceanic change in the slowing and thickening of the glacier for the first time in two decades is strongly supported by the coincident rapid cooling of ocean waters in 2016 and 2017, and by the synchronous recent changes of the three main glaciers around Ilulissat Icefjord (Supplementary Figs. 4 and 6). In a sense, this is a reversal of events of the late 1990s, when the arrival of warmer waters in Disko Bay[8] is hypothesized to have initiated the enhanced melting and retreat of the glacier[9–11,27]. More generally, over the time series we find a near-linear relationship between ocean-induced melting rates and changes in glacier thickness. Indeed, when considered on decadal timescales, the advance and retreat of the glacier's front has been observed to have a close correspondence with ocean temperature variability[39]. In turn, the advance and retreat of the front and the associated modification of the resistance to flow have been shown to be highly influential on the stress regime and dynamic changes of Jakobshavn Isbrae[13,19,40].

Implications for the evolution of Jakobshavn Isbrae

Jakobshavn Isbrae witnessed three decades-long episodes of rapid thinning since the beginning of the twentieth century[41]. The latest started in 1997 and our observations of recent slowing and thickening could signal the end of that episode by 2017. Such episodic course reversals underline the difficulty in projecting contemporary trends into the future to assess glacier contribution to sea-level rise. An earlier study[42] made predictions about the evolution of Jakobshavn using a volume-balance model informed by glacier geometry. Despite the relative simplicity of that model, we can attest from our observations that those predictions were remarkably accurate regarding front positions during the first half of the current decade, and that they foresaw qualitatively the patterns of flow speed changes in that time. We argue that the discrepancies between such predictions and observation occur in large part because ice–ocean interaction is ignored. Ocean-induced melting variability in the case of Jakobshavn is often considered only to the extent of its role in the disintegration of the ice shelf. Yet, our findings demonstrate that the ocean has continuously shaped the dynamic evolution of the glacier since the removal of the ice shelf. Strong ocean–glacier coupling in decades following full ice-shelf collapse has previously been demonstrated in the case of Antarctic glaciers[43].

In the same period since the removal of Jakobshavn's floating ice tongue, its retrograde bed, often invoked as creating a vulnerability to continued retreat, does not appear to offer sufficient explanation of glacier evolution. Grounding lines have been previously observed to re-advance, as in the case of the Dotson–Crosson ice shelves of Antarctica[44], but along relatively flat beds. In contrast, the re-advance of Jakobshavn's front between 2008 and 2009 occurred up an inclined bed (Fig. 2, inset), gaining ~120 m in elevation. Similarly unexpected is the behaviour of the glacier between 2011 and 2017, when the front was mostly grounded on a nearly flat bed suggesting that it would stabilize, but instead exhibited large variability in flow speeds and thickness changes.

Despite the slowdown and thickening we report here, glacier flow still exceeds the velocities of the early 1990s (Supplementary Fig. 6), when the mass balance of the glacier was nearly in equilibrium[45], and continues to contribute to Greenland's net ice mass

loss. Our findings emphasize the necessity of including oceanic and atmospheric variability in projections of Jakobshavn Isbrae's future contribution to sea-level rise. This conclusion adds to the evidence from Antarctica[43,44,46] that, while bed topography exerts principal control on the spatial patterns of grounding line migration, external forcings continue to modulate the rates of retreat or advance.

Online content

Any methods, additional references, Nature Research reporting summaries, source data, statements of data availability and associated accession codes are available at https://doi.org/10.1038/s41561-019-0329-3.

Received: 30 October 2018; Accepted: 14 February 2019;
Published online: 25 March 2019

References

1. Joughin, I., Smith, B. E., Shean, D. E. & Floricioiu, D. Brief communication: further summer speedup of Jakobshavn Isbræ. *Cryosphere* **8**, 209–214 (2014).
2. Bindschadler, R. *Surface Topography of the Greenland Ice Sheet from Satellite Radar Altimetry* (National Aeronautics and Space Administration, Office of Management, Scientific and Technical Information Division, 1989).
3. Howat, I., Joughin, I. & Scambos, T. Rapid changes in ice discharge from Greenland outlet glaciers. *Science* **315**, 1559–1561 (2007).
4. Joughin, I. et al. Continued evolution of Jakobshavn Isbrae following its rapid speedup. *J. Geophys. Res.* **113**, F04006 (2008).
5. Joughin, I. et al. Seasonal to decadal scale variations in the surface velocity of Jakobshavn Isbrae, Greenland: observation and model-based analysis. *J. Geophys. Res.* **117**, F02030 (2012).
6. Moon, T., Joughin, I., Smith, B. & Howat, I. 21st-century evolution of Greenland outlet glacier velocities. *Science* **336**, 576–578 (2012).
7. Enderlin, E. et al. An improved mass budget for the Greenland ice sheet. *Geophys. Res. Lett.* **41**, 866–872 (2014).
8. Holland, D., Thomas, R., de Young, B., Ribergaard, M. & Lyberth, B. Acceleration of Jakobshavn Isbræ triggered by warm subsurface ocean waters. *Nat. Geosci.* **1**, 659–664 (2008).
9. Motyka, R. et al. Submarine melting of the 1985 Jakobshavn Isbrae floating tongue and the triggering of the current retreat. *J. Geophys. Res.* **116**, F01007 (2011).
10. Thomas, R. et al. Investigation of surface melting and dynamic thinning on Jakobshavn Isbræ, Greenland. *J. Glaciol.* **49**, 231–239 (2003).
11. Truffer, M. & Motyka, R. Where glaciers meet water: subaqueous melt and its relevance to glaciers in various settings. *Rev. Geophys.* **54**, 220–239 (2016).
12. Joughin, I., Abdalati, W. & Fahnestock, M. Large fluctuations in speed on Greenland's Jakobshavn Isbræ glacier. *Nature* **432**, 608–610 (2004).
13. Thomas, R. Force-perturbation analysis of recent thinning and acceleration of Jakobshavn Isbræ, Greenland. *J. Glaciol.* **50**, 57–66 (2004).
14. Howat, I. et al. Mass balance of Greenland's three largest outlet glaciers, 2000–2010. *Geophys. Res. Lett.* **38**, L12501 (2011).
15. McMillan, M. et al. A high-resolution record of Greenland mass balance. *Geophys. Res. Lett.* **43**, 7002–7010 (2016).
16. Nick, F., Vieli, A., Howat, I. & Joughin, I. Large-scale changes in Greenland outlet glacier dynamics triggered at the terminus. *Nat. Geosci.* **2**, 110–114 (2009).
17. Felikson, D. et al. Inland thinning on the Greenland ice sheet controlled by outlet glacier geometry. *Nat. Geosci.* **10**, 366–369 (2017).
18. McFadden, E., Howat, I., Joughin, I., Smith, B. & Ahn, Y. Changes in the dynamics of marine terminating outlet glaciers in west Greenland (2000–2009). *J. Geophys. Res.* **116**, F02022 (2011).
19. Bondzio, J. et al. The mechanisms behind Jakobshavn Isbrae's acceleration and mass loss: a 3-D thermomechanical model study. *Geophys. Res. Lett.* **44**, 6252–6260 (2017).
20. Morlighem, M., Rignot, E., Mouginot, J., Seroussi, H. & Larour, E. Deeply incised submarine glacial valleys beneath the Greenland ice sheet. *Nat. Geosci.* **7**, 418–422 (2014).
21. Schoof, C. Ice sheet grounding line dynamics: steady states, stability, and hysteresis. *J. Geophys. Res.* **112**, F03S28 (2007).
22. Gudmundsson, G. Ice-shelf buttressing and the stability of marine ice sheets. *Cryosphere* **7**, 647–655 (2013).
23. Fenty, I. et al. Oceans melting Greenland: early results from NASA's ocean–ice mission in Greenland. *Oceanography* **29**, 72–83 (2016).
24. Studinger, M. *IceBridge ATM L2 Icessn Elevation, Slope, and Roughness* Version 2 (NASA National Snow and Ice Data Center Distributed Active Archive Center, 2014, updated 2017); https://doi.org/10.5067/CPRXXK3F39RV
25. Holland, C., Rosing-Asvid, D., Behrens, A. & Boje, J. Oceanic boundary conditions for Jakobshavn Glacier. Part I: variability and renewal of Ilulissat Icefjord waters, 2001-14. *J. Phys. Oceanogr.* **45**, 3–32 (2015).
26. Gladish, C., Holland, D. & Lee, C. Oceanic boundary conditions for Jakobshavn Glacier. Part II: provenance and sources of variability of Disko Bay and Ilulissat Icefjord waters, 1990–2011. *J. Phys. Oceanogr.* **45**, 33–63 (2015).
27. Straneo, F. & Heimbach, P. North Atlantic warming and the retreat of Greenland's outlet glaciers. *Nature* **504**, 36–43 (2013).
28. Straneo, F. et al. Characteristics of ocean waters reaching Greenland's glaciers. *Ann. Glaciol.* **53**, 202–210 (2012).
29. Jenkins, A. Convection-driven melting near the grounding lines of ice shelves and tidewater glaciers. *J. Phys. Oceanogr.* **41**, 2279–2294 (2011).
30. Xu, Y., Rignot, E., Menemenlis, D. & Koppes, M. Numerical experiments on subaqueous melting of Greenland tidewater glaciers in response to ocean warming and enhanced subglacial discharge. *Ann. Glaciol.* **53**, 229–234 (2012).
31. Carroll, D. et al. The impact of glacier geometry on meltwater plume structure and submarine melt in Greenland fjords. *Geophys. Res. Lett.* **43**, 9739–9748 (2016).
32. Straneo, F. et al. Challenges to understand the dynamic response of Greenland's marine terminating glaciers to oceanic and atmospheric forcing. *Bull. Am. Meteorol. Soc.* **94**, 1131–1144 (2013).
33. Slater, D., Goldberg, D., Nienow, P. & Cowton, T. Scalings for submarine melting at tidewater glaciers from buoyant plume theory. *J. Phys. Oceanogr.* **46**, 1839–1855 (2016).
34. Amundson, J. et al. Ice mélange dynamics and implications for terminus stability, Jakobshavn Isbræ, Greenland. *J. Geophys. Res.* **115**, F01005 (2010).
35. Cassotto, R., Fahnestock, M., Amundson, J., Truffer, M. & Joughin, I. Seasonal and interannual variations in ice melange and its impact on terminus stability, Jakobshavn Isbræ, Greenland. *J. Glaciol.* **61**, 76–88 (2015).
36. Robel, A. Thinning sea ice weakens buttressing force of iceberg mélange and promotes calving. *Nat. Commun.* **8**, 14596 (2017).
37. Van Der Veen, C., Plummer, J. & Stearns, L. Controls on the recent speed-up of Jakobshavn Isbræ, West Greenland. *J. Glaciol.* **57**, 770–782 (2011).
38. Cavanagh, J., Lampkin, D. & Moon, T. Seasonal variability in regional ice flow due to meltwater injection into the shear margins of Jakobshavn Isbrae. *J. Geophys. Res. Earth Surface* **122**, 2488–2505 (2017).
39. Lloyd, J. et al. A 100 yr record of ocean temperature control on the stability of Jakobshavn Isbrae, West Greenland. *Geology* **39**, 867–870 (2011).
40. Vieli, A. & Nick, F. Understanding and modelling rapid dynamic changes of tidewater outlet glaciers: issues and implications. *Surv. Geophys.* **32**, 437–458 (2011).
41. Csatho, B., Schenk, T., Van Der Veen, C. & Krabill, W. Intermittent thinning of Jakobshavn Isbræ, West Greenland, since the Little Ice Age. *J. Glaciol.* **54**, 131–144 (2008).
42. Thomas, R. et al. Accelerating ice loss from the fastest Greenland and Antarctic glaciers. *Geophys. Res. Lett.* **38**, L10502 (2011).
43. Walker, C. & Gardner, A. Rapid drawdown of Antarctica's Wordie Ice Shelf glaciers in response to ENSO/Southern Annular Mode-driven warming in the Southern Ocean. *Earth Planet. Sci. Lett.* **476**, 100–110 (2017).
44. Khazendar, A. et al. Rapid submarine ice melting in the grounding zones of ice shelves in West Antarctica. *Nat. Commun.* **7**, 13243 (2016).
45. Rignot, E., Box, J., Burgess, E. & Hanna, E. Mass balance of the Greenland ice sheet from 1958 to 2007. *Geophys. Res. Lett.* **35**, L20502 (2008).
46. Seroussi, H. et al. Continued retreat of Thwaites Glacier, West Antarctica, controlled by bed topography and ocean circulation. *Geophys. Res. Lett.* **44**, 6191–6199 (2017).

Acknowledgements

The authors acknowledge support from the following sources. A.K.: NASA's Cryospheric Sciences Program; and the Oceans Melting Greenland mission. I.G.F., I.F., O.W. and H.Z.: NASA's Physical Oceanography; Cryospheric Sciences; and Modeling, Analysis and Prediction programmes. C.M.L.: NSF grant ARC-1022472 and NASA's Physical Oceanography programme. H.S.: NASA's Cryospheric Sciences; and Modeling, Analysis and Prediction programmes; and JPL's Research and Technology Development programme. M.R.v.d.B. and B.P.Y.N.: the Netherlands Earth System Science Centre. The authors thank JPL's UAVSAR group for ongoing support for the processing and use of the GLISTIN-A data. The authors thank J. Gobat, A. Huxtable, B. Jokinen and E. Boget (APL-UW) and the captains and crews of R/V *Knorr* and R/V *Atlantis* for their efforts in supporting the Davis Strait array. This work was performed at the Jet Propulsion Laboratory, California Institute of Technology, under contract with the National Aeronautics and Space Administration.

Author contributions

A.K. conceived the study, analysed parts of the data, especially glacier altimetry, prepared some of the figures and wrote most of the paper. I.G.F. analysed parts of the data, especially the oceanography and ECCO ocean state estimates, prepared some of the figures and wrote parts of the paper. D.C. conducted the plume modelling and assisted with some of the figures. A.G. analysed the velocity data and provided the Landsat imagery for front detection. C.M.L. provided Davis Strait mooring data. I.F., O.W. and H.Z. assisted with the production of ECCO ocean state estimates. H.S. advised on glacier dynamics and ice–ocean interactions. D.M. assisted with GLISTIN data calibration and validation. B.P.Y.N. and M.R.v.d.B. contributed the RACMO2.3p2 subglacial discharge data. S.D. coordinated planning and data collection for OMG. J.W. assisted with analysing parts of the oceanography data, assisted with the writing and prepared some of the figures.

Competing interests

The authors declare no competing interests.

Additional information

Supplementary information is available for this paper at https://doi.org/10.1038/s41561-019-0329-3.

Reprints and permissions information is available at www.nature.com/reprints.

Correspondence and requests for materials should be addressed to A.K.

Publisher's note: Springer Nature remains neutral with regard to jurisdictional claims in published maps and institutional affiliations.

Methods

Laser and radar altimetry. Surface elevation changes are obtained from two independent measurements. The ATM laser altimeter[47] that has been flying since 2009 as part of Operation IceBridge and had flown over Greenland since the early 1990s. The data (Level-2 Icessn Elevation, Slope, and Roughness data) have an along-track spacing of 50 m and cover a narrow swath of ~200 m. To find surface elevation changes between repeat ATM observations[44,48] our algorithm considers only points within 25 m from each other. The uncertainty of ATM measurements on grounded ice is assessed to be less than 9 cm (refs. [47,49]). A larger source of uncertainty in finding surface elevation changes from year to year at a given location is the advection of surface features. We estimate this uncertainty from examining the spread of surface elevation difference data located at the same distance from the front to be 1–3 m. The uncertainty diminishes with distance upstream towards the decimetric values expected from the high accuracy of ATM. In the immediate vicinity of the front, the crevassing is so pronounced that surface elevation changes cannot be retrieved. There is no single ATM track that was repeated annually during the study period without any gaps. We therefore find surface elevation changes for the period 2012–2017 along the 2017 ATM track, and those for the period 2005–2011 along the 2011 ATM track. During most years, ATM observations were acquired during spring (exact dates are given in Supplementary Table 1). The thinning or thickening rates are calculated by finding the differences between those measurements from year to year. To find a representative value of yearly surface elevation changes, we calculate the mean thinning or thickening rate for each yearly profile over a section that is 5 km long up-glacier. For each surface elevation change calculation, the 5 km section starts 10 km upstream from the location of the more retreated front of the 2 years being considered. Annual front locations are given in Supplementary Table 1.

GLISTIN-A is a Ka-band airborne radar altimeter[50] that has been flying as part of NASA's OMG mission[23]. Measurements with the GLISTIN instrument obtained during the first 3 years of OMG's airborne campaigns in 2016, 2017 and 2018 provided swath coverage over the entire width of the glacier extending 80 km upstream from the front (Fig. 1c). The GLISTIN data were acquired on 20 March in 2016, on 17 March 17 2017 and on 7 March in 2018. Elevation data are obtained over wide swaths of 10–12 km at a horizontal resolution of 3 m. We smoothed elevation data using a 33 by 33 m mean filter before differencing the digital elevation models of 2016 and 2017 and of 2017 and 2018. GLISTIN's systematic errors from volume scattering average 30 cm under dry snow conditions[51]. We compared the GLISTIN 2016 data (acquired on 20 March) with those of the 2016 ATM (acquired on 16 May) by analysing 16,000 coincident points, which are no more than 25 m apart, on the main trunk of the glacier and in the surrounding areas of slower ice flow. Despite the two-month interval between acquisitions, the mean of the difference between the two data sets was 0.18 m, and the standard deviation from the mean was 2.15 m, demonstrating the relative high accuracy of the GLISTIN data. We find the net contribution of surface processes (mainly precipitation and melting) to observed elevation changes from ATM measurements in areas of slow-moving ice (slower than 200 m yr^{-1}) adjacent to Jakobshavn Isbrae (Supplementary Fig. 5).

In Fig. 2, a running mean smoothing over ~100 m is applied to surface elevation changes. ATM measurements were repeated near-annually along path AA′, and a longer time series of surface elevations and elevation changes (2003–2018), with some gaps, is shown in Supplementary Fig. 2. Elevation changes from GLISTIN observations, shown in Fig. 2 for the years 2017 and 2018, were interpolated along the ATM path.

In Fig. 3a, changes in surface elevation for each year are found relative to the preceding year from ATM observations, and then the values for all points located 10 to 15 km upstream from the front are averaged. For each pair of years that enter into the calculation, the front location used to find the 10–15 km section is the front most upstream of the 2 years. We normalized the averaged surface elevation values by finding the rate of change per day for each pair of years and then multiplying that by 365 days. If observations were made on several dates in a year, we used the earliest of those dates in calculating the number of days separating data acquisition among years. In this plot, the axis of the elevation change was reversed to emphasize the correlation with melting rates. The melting rate for each year is plotted in summer. Surface elevation measurements are made in spring, but the rates of elevation change for each year are shown shifted back in time to the preceding summer to emphasize the correlation with submarine melting. The two time series have a correlation coefficient of −0.67 with a P value of <0.02.

Ice flow velocities. Surface velocities are derived from feature tracking of repeat optical imagery (Landsat 4, 5, 7 and 8; and Sentinel-2a/b) using autonomous Repeat Image Feature Tracking[52]. Velocities are generated for all image pairs with <65 days of separation and have uncorrelated errors of ~30 m yr^{-1} to 300 m yr^{-1}. Velocities were also extracted from NASA's MEaSUREs Greenland Ice Velocity data set[53] derived from TerraSAR-X image pairs and have an uncorrelated uncertainty of ~5 m yr^{-1} to 20 m yr^{-1}.

Glacier front locations and bed topography. We use the same Landsat 7 and 8 imagery data described in the preceding section to locate where the front of the glacier intersects the 2011 or the 2017 ATM tracks in each year (Fig. 1c). We find the Landsat image that is closest in date to the dates of the 2011 or 2017 ATM data acquisitions. The dates of the IceBridge ATM observations and of the front imagery are listed in Supplementary Table 1.

The pixel size of the Landsat Band 8 images is 15 m. As we digitize the front intersection points manually, and given the difficulty sometimes of discerning where the front is due to shadows and fracture, we estimate the uncertainty of front locations to be a few pixels.

Bed topography is from BedMachine Version 3, the most recent version of the data that combines available radar sounding and seismic observations of bed depths beneath Greenland's ice with a mass-conserving model to produce a comprehensive map of bed elevations[54]. Uncertainty in bed elevations in the study region varies between 15 and 100 m.

Oceanographic observations and data assimilation. Ocean temperature data for the Disko Bay analysis were identified using a combination of in situ CTD measurements from the International Council for the Exploration of the Sea Oceanography Data Portal (http://www.ices.dk/marine-data/data-portals/Pages/ocean.aspx) and the World Ocean Database[55]. In addition, airborne expendable and ship-based CTD data from OMG were used in 2015, 2016 and 2017[56]. CTD profiles that fell within the geographic box bounded by 68.8608° N to the south, 54.0208° W to the west, 52.0096° W to the east and 69.3210° N to the north were first averaged to 20-m-depth bins before being averaged with each other. These data were used to infer temperature and salinity changes at the face of the glacier for use in the plume model. North Atlantic subpolar gyre temperatures were identified using a combination of the Estimating the Climate and Circulation of the Ocean (ECCO) global ocean and sea-ice state estimate Version 4, Release 3 (~33 km horizontal resolution in Disko Bay and Davis Strait) and Version 5, Release alpha (~11 km horizontal resolution in Disko Bay and Davis Strait[57–59]) for the time period January 1993–December 2015 and the Roemmich–Gilson Argo Climatology for the time period January 2016–December 2017[60]. We defined the subpolar gyre by selecting the largest closed contour of mean dynamic topography over the gyre region from the ECCO Version 4 product and further restricting the domain to regions where seafloor depths exceed 2,000 m to ensure that Polar Water on the continental shelf was excluded. Differences in subpolar gyre temperatures averaged 0–300 m between the Roemmich and Gilson and ECCO products were generally <0.1 °C during their common time period (2004–2015). Temperatures from the first two years (1992 and 1993) of the ECCO Version 4, Release 3 state estimate are excluded to avoid the period of model spin-up. Importantly, the Disko Bay mooring data after 2015 were not assimilated in the ECCO products.

To construct the Davis Strait temperature and salinity time series shown in Fig. 3e and in the Supplementary Figs, time series with 30 min resolution from moorings C5 at 200 m depth and C6 at 250 m depth in Davis Strait[61] (Fig. 1a) were combined. Observations were collected with MicroCAT conductivity, temperature and pressure recorders. Changes in deployment and instrument issues prevented either mooring from providing a time series for the entire period of interest in both variables. However, overlap during 2013, 2014 and 2015 shows that both moorings sample very similar waters in the boundary current. Moorings were recovered in the summer of 2017.

Modelling submarine melting rates at the front of the glacier. With knowledge of the Jakobshavn Isbrae grounding line depth at its calving front in each year, as well as the expected hydrography in the fjord, it is possible to model an idealized subglacial plume and its interaction with the glacier and surrounding waters[29,31,62]. The flux of buoyant, fresh meltwater emerging from beneath the glacier (Fig. 3c) affects the dynamics of the turbulent plumes that modulate the mass and heat exchanges between the ocean and ice[29]. Water properties at the glacier terminus are assumed to equal those in Disko Bay for depths above 250 m, which is the depth of the sill at the mouth of the fjord. This implies that there is little damping in temperature variability between Disko Bay and the front of the glacier, which has been demonstrated by previous observations[25]. Below that depth, temperature and salinity are assumed to be homogeneous and equal to their values at 250 m (experiments with the values of temperature and salinity varying with depth below 250 m produced higher melting rates still). To estimate subglacial discharge, we use daily surface runoff from RACMO2.3p2, described in detail below. Subglacial discharge is computed over a probability-based catchment area that is delineated by a Monte Carlo approach[31]. A point-source subglacial plume at the front of Jakobshavn is modelled using ocean temperature data collected in 2009[31]. Here we expand on those results by estimating the mean melt rate over each summer when subglacial discharge is active and submarine melting associated with it dominates over ambient melting. Using previously published parameters[33], we estimate that discharge-driven melting dominates over the ambient melting of ice (in the plume region) when subglacial discharge is equal to or greater than 1 $m^3 s^{-1}$. Therefore, we ignore plume-driven melting when discharge is less than 1 $m^3 s^{-1}$. We compute the melting rate as a daily time series. The mean values of the melting rates that we calculate are those of maximum melting, which typically occurs within ~100 m above the grounding line[31]. The depth of the grounding line at which subglacial discharge emerges is from BedMachine Version 3 described above[53]. During summer, if the subglacial discharge is evenly distributed across the width of the terminus as a line plume, instead of emerging from a single subglacial conduit, melting rates are reduced by

roughly a factor of 3. Given this sensitivity, we do not consider the melting rate magnitude to be especially meaningful. However, the interannual variability of the melting rates for both the single-point and line plume simulations is similar.

Runoff and precipitation. Surface mass balance, including runoff, and near-surface temperature are derived from the Regional Atmospheric Climate Model RACMO2, version 3p2 (ref. [63]). For this work, the native horizontal model resolution has been further enhanced from 11 to 5.5 km, and statistically downscaled to 1 km correcting runoff and relevant surface mass balance components for elevation and ice albedo biases, and projected onto the Greenland Ice Mapping Project ice mask and digital elevation model[64]. Compared to previous versions, the RACMO2.3p2 physics package has improved representation of snowfall, drifting snow, surface albedo, melt and runoff leading to improved simulation of the surface mass balance and firn layer structure and refreezing in the accumulation zone[65]. The cumulative surface meltwater production and precipitation time series in the lower reaches of Jakobshavn Isbrae was computed over a geographic box defined by the following pairs of points, starting from the northwest point clockwise: 69.33° N, 50.02° W; 69.37° N, 48.51° W; 69.03° N, 48.44° W; and 68.99° N, 49.92° W.

Data availability

Data are available in the following public repositories, or upon request from the indicated authors. The GLISTIN ice data and the airborne expendable CTD oceanographic data are available at the OMG website: https://omg.jpl.nasa.gov/portal/browse/. The Operation IceBridge ATM data are available from the NSIDC website at https://nsidc.org/data/icebridge/data_summaries.html. The flow speed data used in this study are available from A.G. (Alex.S.Gardner@jpl.nasa.gov) upon request. The Landsat 4, 5, 7 and 8 data, used in inferring glacier flow speeds and front locations, are available at https://cloud.google.com/storage/docs/public-datasets/landsat. The Sentinel-2a/b data used in inferring flow speeds are available at https://cloud.google.com/storage/docs/public-datasets/sentinel-2. The International Council for the Exploration of the Sea oceanographic data are available at http://ices.dk/Pages/default.aspx and http://ices.dk/marine-data/data-portals/Pages/ocean.aspx. The ECCO Version 4 Release 3 and Version 5 Release alpha ocean and sea-ice products are available at http://ecco.jpl.nasa.gov and ftp://ecco.jpl.nasa.gov/Version5/Alpha/. The RACMO2.3p2 data are available from B.P.Y.N. (B.P.Y.Noel@uu.nl) and M.R.v.d.B. (M.R.vandenBroeke@uu.nl) upon request. Bed topography and fjord bathymetry BedMachine Version v3 data are available at http://sites.uci.edu/morlighem/dataproducts/bedmachine-greenland.

References

47. Krabill, W. et al. Aircraft laser altimetry measurement of elevation changes of the Greenland ice sheet: technique and accuracy assessment. *J. Geodyn.* **34**, 357–376 (2002).
48. Khazendar, A., Borstad, C., Scheuchl, B., Rignot, E. & Seroussi, H. The evolving instability of the remnant Larsen B Ice Shelf and its tributary glaciers. *Earth Planet. Sci. Lett.* **419**, 199–210 (2015).
49. Brunt, K. et al. Assessment of NASA airborne laser altimetry data using ground-based GPS data near Summit Station, Greenland. *Cryosphere* **11**, 681–692 (2017).
50. Moller, D. et al. The glacier and land ice surface topography interferometer: an airborne proof-of-concept demonstration of high-precision Ka-band single-pass elevation mapping. *IEEE Trans. Geosci. Remote Sens.* **49**, 827–842 (2011).
51. Hensley, S., Moller, D., Oveisgharan, S., Michel, T. & Wu, X. Ka-band mapping and measurements of interferometric penetration of the Greenland ice sheets by the GLISTIN radar. *IEEE J. Sel. Topics Appl. Earth Observ. Remote Sens.* **9**, 2436–2450 (2016).
52. Gardner, A. et al. Increased West Antarctic and unchanged East Antarctic ice discharge over the last 7 years. *Cryosphere* **12**, 521–547 (2018).
53. Joughin, I., Smith, B., Howat, I., Scambos, T. & Moon, T. Greenland flow variability from ice-sheet-wide velocity mapping. *J. Glaciol.* **56**, 415–430 (2010).
54. Morlighem, M. et al. BedMachine v3: Complete bed topography and ocean bathymetry mapping of Greenland from multibeam echo sounding combined with mass conservation. *Geophys. Res. Lett.* **44**, 11051–11061 (2017).
55. Boyer, T. P. et al. *World Ocean Database 2013* (SilverSpring, accessed July 2018).
56. *OMG* (NASA Jet Propulsion Laboratory, California Institute of Technology, 2018); https://doi.org/10.5067/OMGEV-AXCTD
57. Fukumori, I. et al. *ECCO Version 4 Release 3* (ECCO Consortium, 2017); http://hdl.handle.net/1721.1/110380
58. Forget, G. et al. ECCO version 4: an integrated framework for non-linear inverse modeling and global ocean state estimation. *Geosci. Model Dev.* **8**, 3071–3104 (2015).
59. Zhang H., Menemenlis, D. & Fenty, I. *ECCO LLC270 Ocean-Ice State Estimate* (ECCO Consortium, 2018); http://doi.org/1721.1/119821
60. Roemmich, D. & Gilson, J. The 2004–2008 mean and annual cycle of temperature, salinity, and steric height in the global ocean from the Argo Program. *Progr. Oceanogr.* **82**, 81–100 (2009).
61. Curry, B., Lee, C., Petrie, B., Moritz, R. & Kwok, R. Multiyear volume, liquid freshwater, and sea ice transports through Davis Strait, 2004–10. *J. Phys. Oceanogr.* **44**, 1244–1266 (2014).
62. Carroll, D. et al. Subglacial discharge-driven renewal of tidewater glacier fjords. *J. Geophys. Res. Oceans* **122**, 6611–6629 (2017).
63. Noël, B. et al. Modelling the climate and surface mass balance of polar ice sheets using RACMO2—Part 1: Greenland (1958–2016). *Cryosphere* **12**, 811–831 (2018).
64. Howat, I., Negrete, A. & Smith, B. The Greenland Ice Mapping Project (GIMP) land classification and surface elevation data sets. *Cryosphere* **8**, 1509–1518 (2014).
65. Ligtenberg, S., Kuipers Munneke, P., Noël, B. & van den Broeke, M. Brief communication: Improved simulation of the present-day Greenland firn layer (1960–2016). *Cryosphere* **12**, 1643–1649 (2018).